Int. J. Multiphase Flow Vol. 16, No. 3, pp. 391–406, 1990
Printed in Great Britain.

0301-9322/90 $3.00 + 0.00

ADIABATIC TWO-PHASE PIPE FLOW OF AIR–WATER MIXTURES UNDER CRITICAL FLOW CONDITIONS

M. DEICHSEL and E. R. F. WINTER
Lehrstuhl C für Thermodynamik (Kältetechnik), Technische Universität München, München, B.R.D.

(*Received* 7 *December* 1987; *in revised form* 28 *December* 1989)

Abstract—This investigation deals with the *experimental* determination of the mean velocity ratio of air and water in adiabatic two-phase pipe flows under steady-state critical conditions and with the *analytical* derivation of the mean velocity ratio, mean void fraction and critical mass flux based upon a radial modeling of the flow. An air–water loop was designed and constructed to determine the critical mass flux and the mean velocity ratio with an impulse measurement device as functions of tube diameter and length, pressure and flow quality. Measurements of the radial distribution of total pressure in critical flow at the exit cross-section of the test tube, combined with analytical considerations, yielded radial profiles of density, void fraction and velocity of the phases. These profiles reveal the occurrence of a *locally* homogeneous flow, whereas the *mean* velocity ratio of the flow exceeds the value of unity. Assuming that the local velocities, excepting those near the wall, are equal to the local homogeneous sonic velocity, a subsequent application of an integrational procedure permitted the computation of the mean velocity ratio and the critical mass flux. The results are in good agreement with the experimental data. A parameter variation study proved the applicability of the analytical procedure to the description of critical two-component two-phase flows.

Key Words: critical two-phase pipe flow, velocity ratio, critical mass flux, radial phase distribution, radial velocity distribution, local homogeneous sonic velocity

1. INTRODUCTION

In recent investigations of critical *single-component* two-phase flows (Petry *et al.* 1984) a number of problems associated with phase transition and phase distribution, together with the ensuing velocity ratio, remained unresolved. In order to clarify these open questions a research project was initiated to study critical *two-component* two-phase flows of air–water mixtures in pipes of small diameters, reflected in a report by Winter & Deichsel (1988). Based upon prior experience gained in connection with the design, construction and operation of a freon-loop, an air–water flow facility was developed. Contrary to the problems associated with phase transition in single-component two-phase flows, two-component two-phase flows only raise questions concerning the occurrence of hydrodynamic non-equilibrium, expressed in terms of the velocity ratio, and none regarding phase transition and thermodynamic non-equilibrium of the flow system.

2. PHYSICAL MODEL

The physical model of the adiabatic two-component critical flow under study, which provides the basis for the development of the *one-dimensional* steady-state conservation equations, is shown in figure 1. A sufficiently high pressure difference between the supply vessel and the plenum chamber causes the two-phase flow to become critical in the exit cross-section of the test tube.

The test pipe is supplied with constant water and air mass flow rates of varying ratios, $\dot{m}_L$ and $\dot{m}_G$, under variable supply pressures, p_0, at a fixed ambient temperature, T_0. Particular critical flow conditions in the exit plane, A_E, of the system are achieved by adequately reducing the chamber pressure, p_∞, while keeping the supply pressure, p_0, at a desired level. Leaving the pipe, the critical two-phase flow forms a jet which is deflected perpendicularly to the flow direction by the rotationally symmetrical impulse device, allowing the measurement of the total momentum of the flow in terms of a reaction force, $F_{R,z}$. This concept was first employed in form of an "impulse plate" by Giffen & Crang (1946). Conditions in the entrance and exit sections of the test pipe are denoted

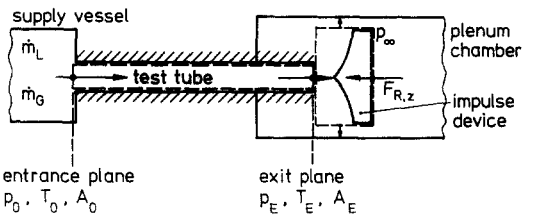

Figure 1. Physical model.

by the subscripts, 0 and E, respectively. In figure 1 two system boundaries are shown. The one within the test tube encompasses an open adiabatic system for which the mass continuity equation becomes

$$\dot{m}_L + \dot{m}_G = \text{const.} \quad [1]$$

The other boundary circumscribes the impulse device and the region of the deflected two-phase jet. For this boundary, with the exception of the very discharge (pipe) area, A_E, the acting static pressure is considered to be the constant pressure of the plenum chamber, p_∞. The momentum equation in the axial direction for this open system reduces to the resultant force balance:

$$F_{R,z} = (\dot{m}_L \cdot \bar{w}_L + \dot{m}_G \cdot \bar{w}_G) + A_E(p_E - p_\infty), \quad [2]$$

where the $\bar{w}$ denote the mean phase velocities. Introducing the definition for the mean velocity ratio, $\bar{S}$, of the critical two-phase flow in the exit cross-section,

$$\bar{S} = \frac{\bar{w}_G}{\bar{w}_L}, \quad [3]$$

into the equation for the force balance, and recognizing that the exit cross-sectional area of the flow can be determined according to

$$A_E = \frac{\dot{m}_L}{(\bar{w}_L \rho_L)} + \frac{\dot{m}_G}{(\bar{w}_G \rho_G)}, \quad [4]$$

a quadratic equation is obtained, which is in agreement with similar expressions presented by Vance (1962) and Klingebiel & Moulton (1971):

$$\bar{S}^2 + \bar{S}\left[\frac{A_E^2 \rho_L}{\dot{m}_G}\frac{(p_E - p_\infty)}{\dot{m}_L} - \frac{A_E}{\dot{m}_G}\frac{F_{R,z}\rho_L}{\dot{m}_L} + \frac{\dot{m}_G \rho_L}{\dot{m}_L \rho_G} + \frac{\dot{m}_L}{\dot{m}_G}\right] + \frac{\rho_L}{\rho_G} = 0. \quad [5]$$

Solution of [5] for the *mean* velocity ratio, $\bar{S}$, requires the experimental determination of the unknown quantities in appropriate experiments.

3. EXPERIMENTAL FACILITY

An air–water two-phase flow facility, the schematic diagram of which is given in figure 2, was designed and constructed. The test facility consists of an open air "loop" and a closed water loop.

Two compressors supply an adequate mass flow rate of air at a sufficiently high pressure. The gas passes through a filter and continues through a pressure-reducing valve for pre-adjustment of the desired supply pressure. Then the air flows through a heater where its temperature is increased to the ambient level. An orifice type flow meter, together with a pneumatic valve, are used to adjust its flow rate in accordance with the desired constant supply pressure level, p_0, ranging from 7 to 25 bar.

A reciprocating pump supplies a filtered water flow of required rate and pressure. The pressure surges are dampened out in pressure-equalizing vessels. Flow rate and supply pressure are regulated by means of a pneumatic valve and a turbine flow meter in such a way that, after combining the two flows in the mixing chamber, the predetermined supply pressure, p_0, and the flow quality, $\dot{x}$, remain constant.

A mesh wire structure, installed in the mixing chamber, insures that a homogeneous two-phase flow mixture of constant flow quality, $\dot{x}$, pressure, p_0, and temperature, T_0, enters the interchangeable test tubes. Each test tube is provided with pressure taps (dia 0.1–0.3 mm) for determination of the static pressure distribution in the flow direction and with thermocouples for measurement of the wall temperature. The spacings between the pressure and temperature probes are reduced towards the exit of the test tubes, in order to acquire sufficiently accurate data. Leaving the exit plane of the test tube, the flow develops into a two-phase jet impinging symmetrically upon the conically-shaped impulse vane deflecting the jet perpendicularly to its axis. The expanded two-phase jet leaves the plenum chamber, passing through two flexible hoses connected to a blow-off tank that is fitted with a relief valve for release of the air into the atmosphere. The valve is manually adjustable and serves to control the pressure, p_∞, in the plenum chamber. The water is returned to the supply tank by way of a float valve.

The mixing chamber, test tube and plenum chamber are mounted on a tilting rig having an angular freedom of 90°. All other components of the facility are locked in place. A data acquisition system, assisted by a computer for data reduction, processes the relevant experimental data and solves [5] for the mean velocity ratio, $\bar{S}$. It is essential to recognize, that the static pressure in the exit cross-section of the test tube cannot be measured directly and that it has to be obtained indirectly from pressure measurements along the tube wall and within the expanding jet. An exponential spline routine and an interpolation and extrapolation procedure yield the acting exit pressure, p_E, from the measured values. Under adiabatic flow conditions it was found that the temperature of the flow in the exit cross-section is identical with that measured at the tube wall 5 mm upstream of the exit plane.

The schematic diagram in figure 3 illustrates the impulse and pressure measurement device, the purpose of which is threefold:

- measurement of the reaction force, $F_{R,z}$, for determination of the total momentum of the critical two-phase flow;
- measurement of the static pressure distribution, $p(z)$, in the axial direction of the flow to assist in determining the exit pressure, p_E; and
- measurement of the radial total pressure distribution, $p_{tot}(r)$, in the exit plane, revealing the radial distribution of the local momentum.

To accomplish these tasks, the base of the device, not shown in figure 3, is mounted on a remotely controlled, motor-driven, three-dimensional traversing mechanism, permitting a precise positioning of the probes. The interchangeable nose cones, which are shaped to follow the streamlines of an incompressible stagnation point flow, have base diameters of 70 and 110 mm.

The device for recording the reaction force is attached to a load cell, the sensitivity of which is ~0.4%, generating a signal which is a measure for the momentum acting on it.

The measurement of the static pressure distribution in the flow direction is carried out using another, cone-like device (figure 3). This static pressure sensing probe is fitted with a hollow needle

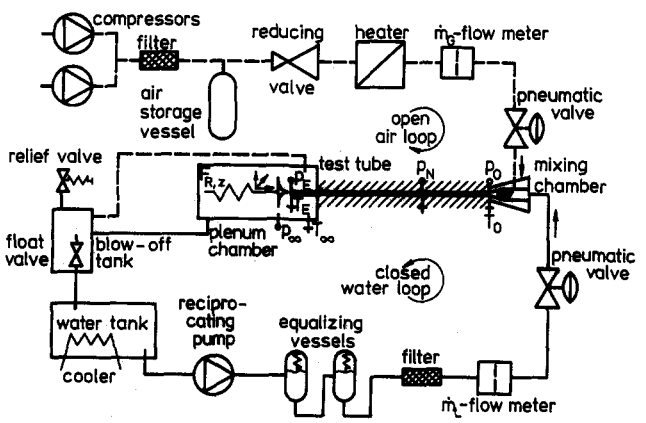

Figure 2. Schematic layout of the two-phase flow facility.

(dia 0.45 mm) at its head, which has a pressure tap (dia 0.1 mm) on the side to measure the static pressure, p_E, in the exit cross-section and the axial static pressure distribution, $p(z)$, in the expanding free jet.

A second head, also fitted with a hollow needle, has a pressure tap (dia 0.15 mm) at its tip for recording the radial total pressure distribution, $p_{tot}(r)$, within the exit cross-section.

During the measurements, the connecting flexible metal tubes (i.d. 1.5 mm) between the pressure tap and the transducer are filled with water. The applicability and reliability of the three measurement techniques, measurement of the reaction force and of the static pressure, together with the total pressure distributions were tested with single-phase water and air flows. Deviations between measured and predicted values under single-phase flow conditions for the reaction force did not exceed 0.014 N in water flows (relative accuracy 0–2%) and 0.175 N in air flows (relative accuracy 0–8%), whilst the deviation between measured and calculated local dynamic pressures in the center of the exit plane in both cases did not surpass 3%.

4. EXPERIMENTS

Critical flow conditions had to be verified prior to the acquisition of experimental data. Attainment of critical conditions was based on the two well-known criteria, which are illustrated in figures 4a, b:

- Once a critical mass flow rate $\dot{m}_{cr} = (\dot{m}_L + \dot{m}_G)_{cr}$ is reached at a preset constant supply pressure, p_0, and a constant flow quality, $\dot{x}$, a subsequent decrease in the pressure, p_∞, in the plenum chamber does not increase the flow rate any further. This is shown qualitatively in figure 4a for two different constant supply pressures $p_{0,I}$ and $p_{0,II}$ and constant flow qualities, $\dot{x}$, in response to an increase in the pressure drop $(p_0 - p_\infty)$.
- In the exit cross-section of the test tubes the fluid velocity equals the sonic flow velocity, i.e. the static pressure in the exit region of the tube does not react to a further lowering of the pressure, p_∞, in the plenum chamber. A typical measurement for this criterion is displayed qualitatively in figure 4b. The development over time of both mass flow rates and several static pressure values is depicted in response to a stepwise decrease in the pressure in the plenum chamber. Critical conditions are achieved when the static pressure in the last tap, $p_{(-1)}$, does not react any longer to the pressure decrease in the plenum chamber. Notice the last pressure step in figure 4b, in which the dashed line indicates the range for which occurrence of the critical flow condition in the exit plane of the test tube is assumed.

It is obvious that the pressure criterion is more readily recognizable than that of the asymptotic behavior of the flow rate.

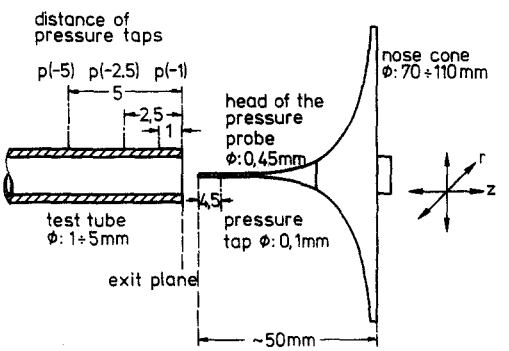

Figure 3. Impulse and pressure measurement device.

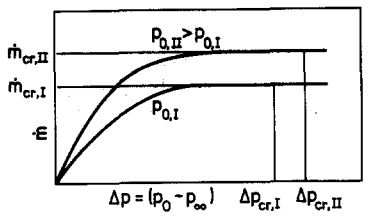

Figure 4a. Criterion for the critical mass flow rate

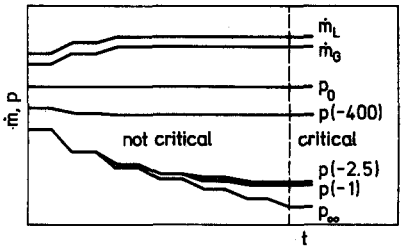

Figure 4b. Mass flow rates and static pressure development in response to a reduction in chamber pressure. The values in parentheses identify the position of the pressure taps.

5. EXPERIMENTAL RESULTS

Several typical static pressure profiles, $p(z)$, measured along the axis of the flow in the end section of the test tube and in the expanding free jet are displayed in figure 5. The pressure distributions reveal an increase in the pressure gradient reaching maximal values in the vicinity of the exit plane with increasing mean flow qualities. The static pressure of the free jet with flow qualities >0.1 and mean void fractions >0.85 in the exit plane falls significantly below the chamber pressure, p_∞, thereby forming well-defined standing pressure waves, also observed by Faletti (1959) and Klingebiel (1964). The pressure profiles disclose a downstream distance of approx. $D/2$ from the exit cross-section at which the static pressure in the axis of the expanding jet for the first time equals the plenum chamber pressure, p_∞. Knowledge of both, distance from the exit plane and of the chamber pressure, are prerequisites for the determination of the exit pressure, p_E, by means of mathematical routines. This holds true because the axial pressure profiles, as shown in figure 5, can only be measured in a few significant test runs. In all other cases the exit pressure, p_E, had to be derived mathematically by either interpolation or exponential spline routines from the measured static pressure in the exit section of the test tube (figure 3) and the acting chamber pressure at the distance $D/2$.

Measurements of the radial distribution of the static pressure in the exit cross-section show only a very weak decrease towards the wall. For this reason a constant static pressure, p_E, throughout the exit cross-section is assumed for the subsequent data reduction.

6. DATA REDUCTION

The data reduction unit processes the acquired data of a particular experiment and the pertinent fluid properties together with the solution procedure for [5]. Typical sets of the resulting data

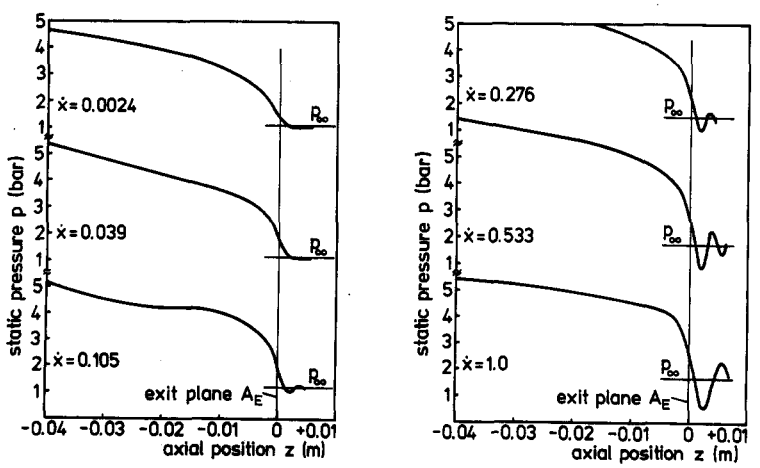

Figure 5. Axial static pressure profiles ($p_0 \sim 15$ bar, $D = 0.003$ m, $L = 0.468$ m).

contain the mean critical velocity ratio, $\bar{S}$, and its dependence on the mean void fraction, $\bar{\epsilon}$, in the exit cross-section as function of the flow quality, which are displayed in figures 6a and 6b. In this context it should be mentioned that the pressure- and temperature-dependent mean void fraction, rather than the flow quality which is constant over the whole length of the pipe, is the more significant two-phase flow parameter for the description of the critical flow behavior in the exit cross-section. Another exemplary set of reduced data is shown in figures 7a and 7b, wherein the critical mass flux, G, is plotted vs the mean void fraction and the flow quality. In all diagrams it is noteworthy that, for a coherent set of data obtained with one constant supply pressure, the exit pressure varies by a factor of about 2 due to frictional effects.

Table 1 is a listing of parameter ranges within which the current experiments were performed by Winter & Deichsel (1988). Summarizing the results of a large number of these experiments demonstrates that the *mean critical velocity ratio*:

- varies with the mean void fraction, while approaching unity for the two limiting values ($\bar{\epsilon} \to 0$ and $\bar{\epsilon} \to 1$);
- reaches a maximum under critical flow conditions in the range, $0.9 < \bar{\epsilon} < 0.95$;
- becomes independent of pipe diameters $D \geqslant 3$ mm, however, increases with a decreasing diameter from $D = 3$ to $D = 1.1$ mm;
- is invariant for length over diameter ratios $L/D \geqslant 156$;
- depends weakly upon length over diameter ratios $156 > L/D \geqslant 5.5$; and
- decreases with increasing exit pressure, p_E.

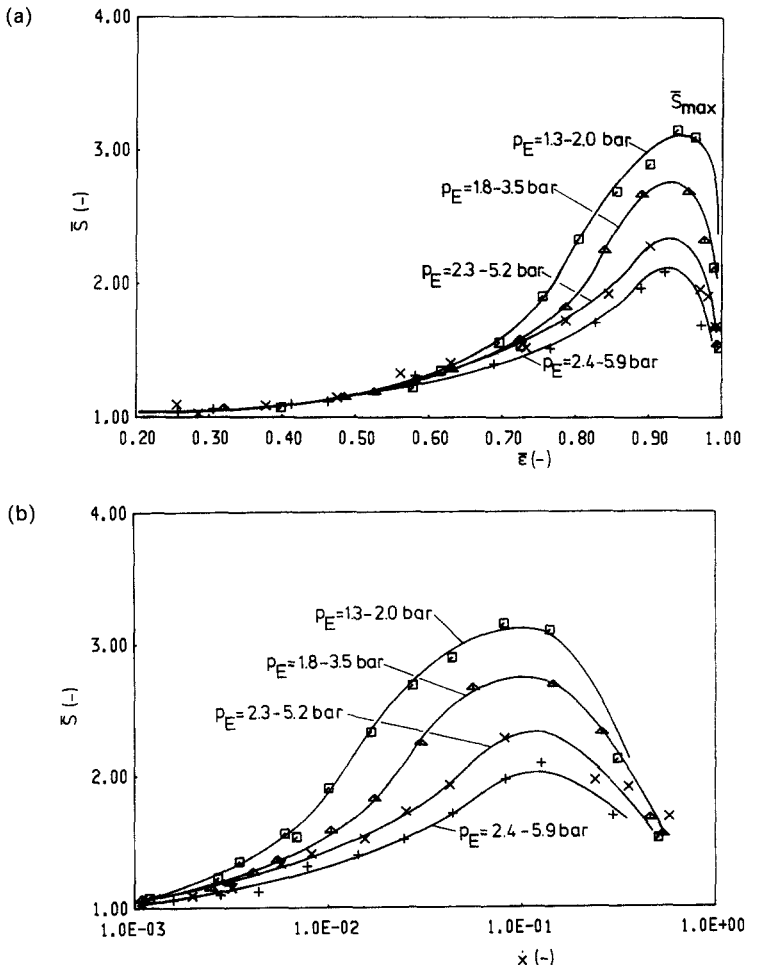

Figures 6a, b. Mean critical velocity ratio related to the mean void fraction in the exit cross-section and the flow quality (□ $p_0 \sim 10$ bar, △ $p_0 \sim 15$ bar; × $p_0 \sim 20$ bar, + $p_0 \sim 25$ bar; $L/D = 156$, $D = 0.003$ m, $L = 0.468$ m, $T \sim 293$K).

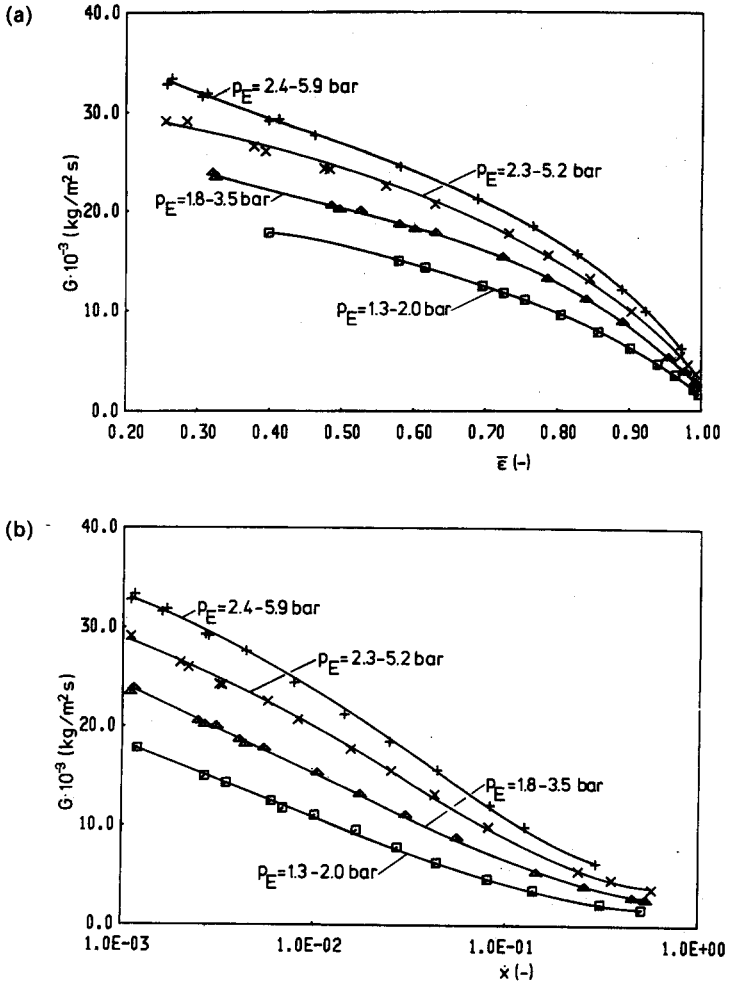

Figures 7a, b. Critical mass flux related to the mean void fraction in the exit cross-section and the flow quality (□ $p_0 \sim 10$ bar, △ $p_0 \sim 15$ bar, × $p_0 \sim 20$ bar, + $p_0 \sim 25$ bar; $L/D = 156$, $D = 0.003$ m, $L = 0.468$ m, $T \sim 293$K).

The flow patterns observed range from dispersed bubble to dispersed spray flows undergoing continuous transitions from one regime to another. The sizes of bubbles and droplets do not exceed a few hundredths of a millimeter, caused by high velocities and the associated shear stresses.

7. TOTAL PRESSURE DISTRIBUTION IN THE TUBE EXIT

Numerous measurements of *total* pressure profiles in the exit area of the test tubes were performed, covering the entire range of mean void fractions from $\bar{\epsilon} = 0$ (subcritical pure water flow) to $\bar{\epsilon} = 1$ (critical pure air flow), in order to shed some light upon the behavior of the critical mean velocity ratio. Representative results in terms of reduced *dynamic* pressure profiles, $\hat{p}_{dyn}(r) = \hat{p}_{tot}(r) - p_E$ are plotted in figure 8, in which the scale of the ordinate is subdivided with regard to each profile. The shape of the profiles varies from a turbulent one, for pure water with a maximum dynamic pressure in the center of the flow, via those with a minimum in the center and a maximum close to the wall and again to profiles approaching that of pure air flow with a

Table 1. Experimental parameters (rounded)

Parameter	Symbol	Value	Unit
Diameter	D	0.0011, 0.0019, 0.003, 0.005	m
Length/diameter	L/D	5.5, 156, 273, 500	—
Supply pressure	p_0	7, 10, 15, 20, 25	bar
Flow quality	$\dot{x}$	0.002–0.5	—
Orientation		horizontal/vertical	

maximum in the center. The motivation for this particular study of local dynamic pressures in the exit cross-section was the desire to clarify the interdependence of the local phase distribution, $\hat{\epsilon}(r)$, the local velocity ratio, $\hat{S}$, and the mean velocity ratio, $\bar{S}$. Since the critical two-phase flow has a velocity maximum in the center and the local dynamic pressure depends upon the local values of density and velocity of both phases and upon the local void fraction, $\hat{p}_{dyn} = f(\hat{\rho}_G, \hat{w}_G, \hat{\rho}_L, \hat{w}_L, \hat{\epsilon})$, the working hypothesis can be established that the density of the flow assumes a maximum at the wall and that it decreases towards the axis. For the description of this type of flow, the dispersed two-phase flow model with radial density and void fraction distributions, first presented by Behringer (1936) and later improved by Zuber & Findlay (1965), is successfully adapted to dispersed critical flows.

As shown schematically in the modeling procedure, depicted in figure 9, this novel application allows the evaluation of the dynamic pressure profile for subsequent computation of the radial velocity profile of the flow. The iterative modeling procedure consists of a superposition of the *measured* dynamic pressure distribution and of the *assumed* distribution for the local void fraction, according to

$$\hat{\epsilon}(r) = \hat{\epsilon}_{r=0} - (\hat{\epsilon}_{r=0} - \hat{\epsilon}_{r=R})\left(\frac{r}{R}\right)^n. \qquad [6]$$

The partition exponent, n, in the above equation determines the variation of the gradient of the local void fraction between the boundary values at the wall, $r = R$, and in the center of the flow, $r = 0$. The following two equations,

$$\hat{p}_{dyn} = \frac{1}{2}\left[\hat{\epsilon}\rho_G \hat{w}_G^2 + \hat{J} \cdot (1-\hat{\epsilon})\rho_L \left(\frac{\hat{w}_G}{\hat{S}}\right)^2\right] \qquad [7a]$$

and

$$\hat{p}_{dyn} = \frac{1}{2}\hat{J}'\left[\hat{\epsilon}\rho_G \hat{w}_G^2 + (1-\hat{\epsilon})\rho_L \left(\frac{\hat{w}_G}{\hat{S}}\right)^2\right], \qquad [7b]$$

are used to calculate the phase velocity distributions from the measured dynamic pressure. In these equations a local velocity ratio, $\hat{S}$, must be assumed, whereas for the momentum exchange factor $\hat{J}$, correlations given by Adorni *et al.* (1961) and Reimann (1983), as well as our own correlation for $\hat{J}'$ adjusted to critical flow, were employed:

$$\begin{aligned} 0 \leqslant \hat{\epsilon} \leqslant 0.245: \quad & \hat{J}' = 1.0 + 0.404 \cdot \hat{\epsilon} \\ 0.245 < \hat{\epsilon} \leqslant 1.0: \quad & \hat{J}' = 0.9718 + 4.3125 \cdot \hat{\epsilon} - 38.7393 \cdot \hat{\epsilon}^2 \\ & \quad + 130.5003 \cdot \hat{\epsilon}^3 - 161.5894 \cdot \hat{\epsilon}^4 \\ & \quad + 65.8695 \cdot \hat{\epsilon}^5. \end{aligned} \qquad [8]$$

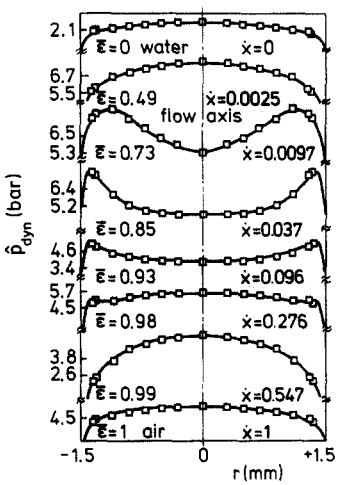

Figure 8. Dynamic pressure profiles (p_0 for the two-phase flow profiles: ~15 bar, $D = 0.003$ m, $L = 0.468$ m, $T \sim 293$K).

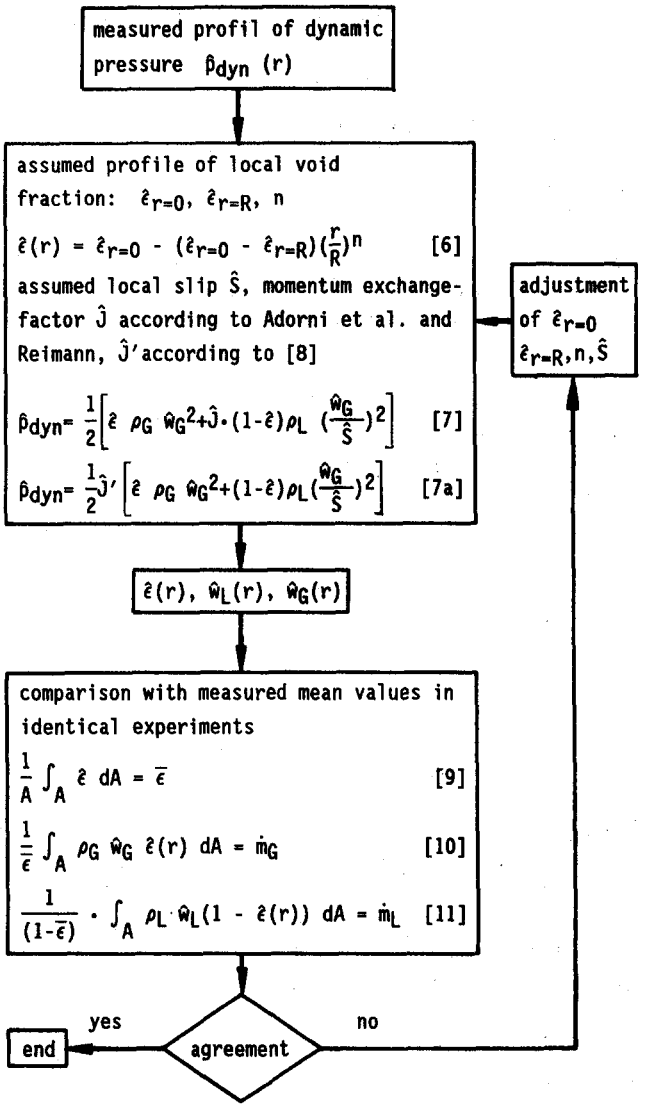

Figure 9. Iterative modeling procedure.

Subsequent to preselection and optimization of the boundary conditions at the wall and in the center of the flow, of the partition exponent and the local velocity ratio, an integration is performed to yield the average void fraction

$$\frac{1}{A}\int_A \hat{\epsilon}\,\mathrm{d}A = \bar{\epsilon} \qquad [9]$$

and the mass flow rates

$$\frac{1}{\bar{\epsilon}}\int_A \rho_G \hat{w}_G \hat{\epsilon}(r)\,\mathrm{d}A = \dot{m}_G \qquad [10]$$

and

$$\frac{1}{(1-\bar{\epsilon})}\cdot\int_A \rho_L \hat{w}_L[1-\hat{\epsilon}(r)]\,\mathrm{d}A = \dot{m}_L. \qquad [11]$$

Integration of the preceding equations is done in such a way that the computational results reach agreement with the mean data of the corresponding experiments described in section 6. In the

course of the integrational procedure attention was paid to satisfying meaningful physical requirements so that:

- the local void fraction between the wall and the center of the tube is continuously rising or becoming constant, respectively;
- the local velocity at the wall is zero;
- the local velocity between the wall and the center of the tube is continuously rising or becoming constant, respectively;
- the local velocity in two-phase flows with a void fraction >0.15 does not surpass the sonic velocity of the corresponding critical pure air flow; and
- the value of the local velocity ratio is always less than that of the mean velocity ratio.

The salient feature of this procedure is the fact that in all cases investigated the physically most plausible results are obtained by equating the local velocity ratio with unity, $\hat{S} = 1$, implying that the flow is locally homogeneous. This outcome agrees well with observations cited by Langner (1978) and Adorni *et al.* (1961). According to their findings, the local velocity ratio approaches unity for small droplets in continuous gas flows and for small bubbles in continuous liquid flows. Under the condition of a velocity ratio, $\hat{S} = 1$, both local velocities assume the same value and become equal to the local two-phase flow velocity according to

$$\hat{w}_{2ph} = \hat{\epsilon}\hat{w}_G + (1 - \hat{\epsilon})\hat{w}_L . \qquad [12]$$

8. SEMI-ANALYTICAL RESULTS

Results for the local two-phase velocity, $\hat{w}_{2ph}$, under critical flow conditions, plotted vs the radius, r, of a test tube (i.d. 3 mm), are presented in the left half of figure 10 for different mean void fractions in the exit cross-section. As would be expected, local velocities and void fractions rise simultaneously, especially, in the center of the flow. Also, the difference between velocities in the center of the flow and near the wall increases with rising mean void fraction, thus explaining the increase in the *mean* velocity ratio displayed in figures 6a and 6b. However, for the mean void fraction, $\bar{\epsilon} > 0.9$–0.95, the velocity rise in the vicinity of the wall is more pronounced than in the center of the flow, causing the decrease in the measured mean velocity ratio.

A comparison of the local velocity profiles for several experiments is displayed in the right half of figure 10. This graph demonstrates the good agreement and consistency of the velocity data derived from the measured dynamic pressures by using [8] and different conversion functions given by Adorni *et al.* (1961) and Reimann (1983). It should be emphasized that for the different computations only the conversion function is changed, whereas the radial distribution of the void fraction is kept the same for each experiment.

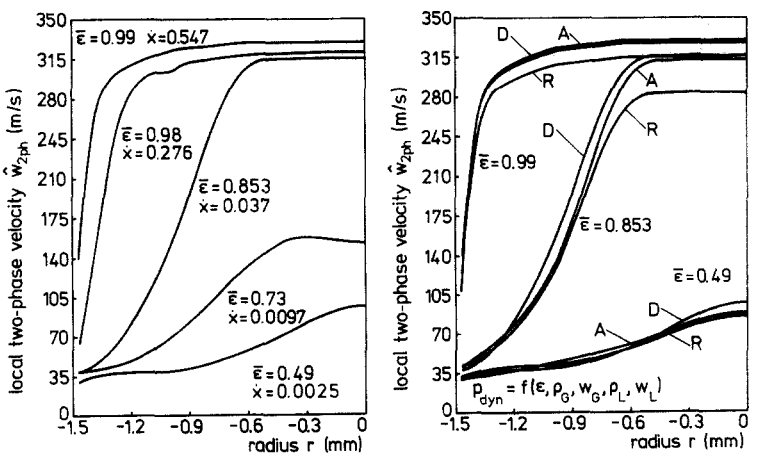

Figure 10. Radial velocity profiles deduced from experimental data (l.h.s.) compared with deduced data using different conversion functions from Adorni *et al.* (1961) (A) and Reiman (1983) (R), and the current correlation [8] applied to critical flow (D) ($p_0 \sim 15$ bar, $D = 0.003$ m, $L = 0.468$ m, $T \sim 293$K).

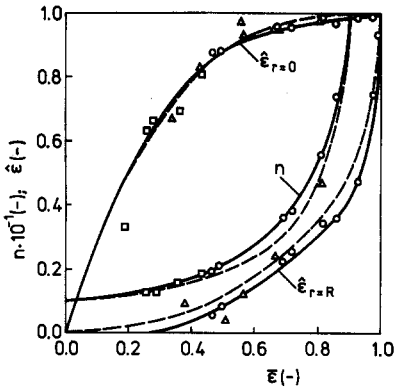

Figure 11. Functional relationship between the local and mean void fraction, and the partition exponent [○ $D = 0.003$ and 0.005 m, △ Nabizadeh-Arahgi (1977), □ Petrick (1962)].

Additional results are shown in figure 11, in which the functional relationships between the wall ($r = R$) and the centerline ($r = 0$) local void fractions, together with the partition exponent and the mean void fraction, are displayed. Furthermore, the graph contains data given by Petrick (1962) and Nabizadeh-Arahgi (1977) for other fluids, however, under noncritical flow conditions. Approximations (dashed lines in figure 11) for the two boundaries and for the partition exponent derived from these data and depending upon the mean void fraction are given by the following equations:

$$\hat{\epsilon}_{r=R} = 1 - (1 - \bar{\epsilon})^{(\bar{\epsilon}/3)}, \qquad [13]$$

$$\hat{\epsilon}_{r=0} = 1 - (1 - \bar{\epsilon})^{3.1} \qquad [14]$$

and

$$n = \frac{1.015}{(1.015 - \bar{\epsilon})}. \qquad [15]$$

In the range of $\bar{\epsilon} < 0.75$ the results obtained with [13]–[15] show good agreement with the findings for air–water flows at low velocities reported by van der Welle (1985), who did not account for the increase in the local void fraction at the wall.

Although no experiments were performed in subcritical two-phase flows, a rather good agreement was obtained between the results of the proposed modeling yielding the radial distribution of the void fraction and the experimental data given by Petrick (1962), Nabizadeh-Arahgi (1977) and van der Welle (1985). Therefore, this novel method can also be applied to the calculation of radial distributions of the void fraction in non-critical flows, provided the flow is *dispersed.*

9. HOMOGENEOUS SONIC VELOCITY

Experimental data, together with computations, have suggested that the velocities of the two phases are locally identical. Consequently, there does exist a locally homogeneous flow system, and since the flow is critical, its local two-phase velocity must equal the local homogeneous sonic velocity, $\hat{a}_h$. This observation is reflected in figure 12, in which both velocities, the one derived from measurements and the other calculated according to the model given by Nguyen & Winter (1981), are shown for comparison at three significantly different mean void fractions. Disregarding the values close to the wall, the agreement between both types of results is remarkable, implying that the homogeneous sonic velocity can be used as a limiting approximation of the local two-phase velocity under critical conditions. The diagram also contains an insert (r.h.s.) of the homogeneous sonic velocity plotted against the void fraction, computed with the flexible wall model given by Nguyen & Winter (1981). From this, it follows that the sonic velocity increases with pressure (here p_E), while the limiting sonic velocities for $\epsilon = 0$ (pure water) and $\epsilon = 1$ (pure air) remain constant. This particular feature explains the pressure-dependent decrease in the mean velocity ratio, as

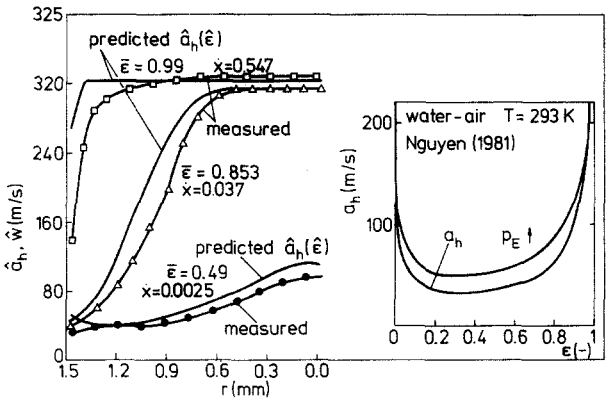

Figure 12. Comparison of predicted local homogeneous sonic velocities with measured velocities.

shown in figures 6a and 6b, the reason being the decrease in the velocity difference between the core flow and the one close to the wall.

In single-phase, one-component pipe flows the sonic velocity is constant over the cross-section of the conduit and its mean value equals the local value in the absence of radial distributions in temperature and properties. For calculation of the maximum mean flow velocity no integrational procedure is needed. In contrast to the behavior of this type of flow, in two-phase flows the sonic velocity depends upon the local properties and especially on the local void fraction. Since the void fraction varies over the cross-section of this flow, the two-phase sonic velocity also varies and because the relationship between the two quantities is not linear, as demonstrated in the right half of figure 12, a computation with average values is not permissible, thus an integrational procedure has to be applied.

Once, the radial distribution of the local void fraction is known from [6] and [13]–[15], it is possible to compute the radial distribution of the local two-phase velocity with the help of the void fraction and the pressure-dependent local homogeneous sonic velocity. The results of these computations with the mean void fraction as parameter are shown in the left half of figure 13. In this context it must be stressed that for mean void fractions < 0.6, the computed local homogeneous sonic velocities show an increase near the wall. Since such an increase is physically impossible, the 1/7-power-law must be employed to predict the true velocity distribution in the wall regions, as illustrated in the right half of figure 13. For that reason, the local two-phase velocity close to the wall in [12] is substituted by the 1/7-power-law velocity distribution.

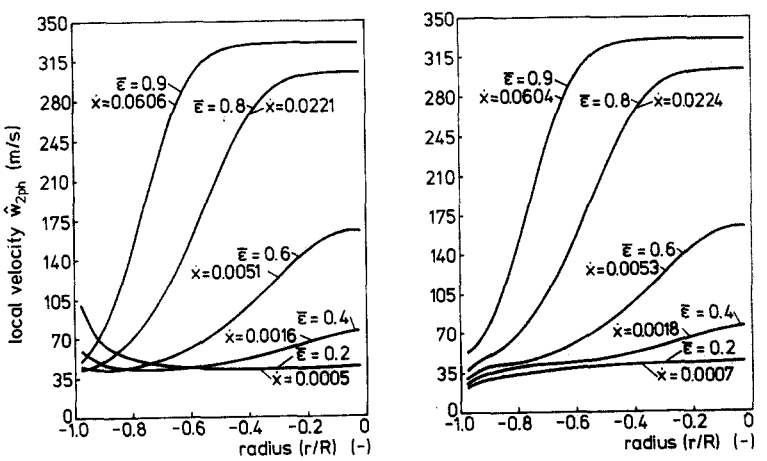

Figure 13. Radial velocity profiles computed with the current model for an air–water system ($p = 2$ bar, $T = 293$K).

The mean velocity ratio under critical flow conditions can be derived from

$$\bar{S} = \frac{\int_A \hat{a}_h(\hat{\epsilon}) \cdot \hat{\epsilon}(r)\, dA}{\int_A \hat{a}_h(\hat{\epsilon}) \cdot [1 - \hat{\epsilon}(r)]\, dA} \cdot \frac{(1-\bar{\epsilon})}{\bar{\epsilon}}. \qquad [16]$$

Integrating the local void fraction related sonic velocity terms in [16] within the identified limits shown in figure 11, and given by [13]–[15], and taking into account that the local velocity has to go to zero at the wall, the interdependence between the mean velocity ratio and mean void fraction can be demonstrated for three different exit pressures, as shown in figure 14. If the 1/7-power-law and the wall condition of zero velocity were not taken into account, the local velocity in the proximity of the wall would have risen to a maximum, yielding a mean velocity ratio of <1 and very high values for the critical mass flux which were not measured in the course of the experiments.

A further development in the current modeling procedure yields the following expression for the critical mass flux:

$$G = \frac{1}{A}\left\{\rho_G \int_A \hat{a}_h(\hat{\epsilon})\hat{\epsilon}(r)\, dA + \rho_L \int_A \hat{a}_h(\hat{\epsilon})[1 - \hat{\epsilon}(r)]\, dA\right\}. \qquad [17]$$

This equation provides a computational tool for the prediction of the critical mass flux, which is plotted vs the mean void fraction with exit pressures as a parameter in figure 15. Predictions for the mean velocity ratio and critical mass flux coincide quite well with the experimental findings.

It is remarkable that the calculated velocity profiles under critical flow conditions do not match the profiles called for by the distribution function, $(y/r)^{1/m}$. However, this disagreement is not a contradiction, because profiles of this type were only observed in subcritical steady-state flows with low axial pressure gradients. From such initially subcritical velocity profiles, $(y/r)^{1/m}$, the flow accelerates while approaching critical velocities, especially, in the center of the flow. Locally the velocity is limited by the sonic velocity, which depends upon the local void fraction. Solely in the vicinity of the wall, where the local velocity must approach zero, and in case of critical two-phase flows having mean void fractions <0.6, these conditions no longer hold true. Because of the different velocity profiles and of the variation in the radial phase distribution, particularly in the range of small mass fluxes in critical and non-critical flows, the functional relationship between the *mean* velocity ratio and *mean* void fraction for non-critical flows has to be modified. In addition to these effects occurring in non-critical flows the acting shear stress decreases, causing an increase in the size of bubbles and droplets, so that a local velocity ratio, $\hat{S} > 1$, must be considered, as for instance, has been observed by Adorni *et al.* (1961) and Langner (1978). Finally, it can be summarized that especially for dispersed undercritical two-phase flows, the radial phase

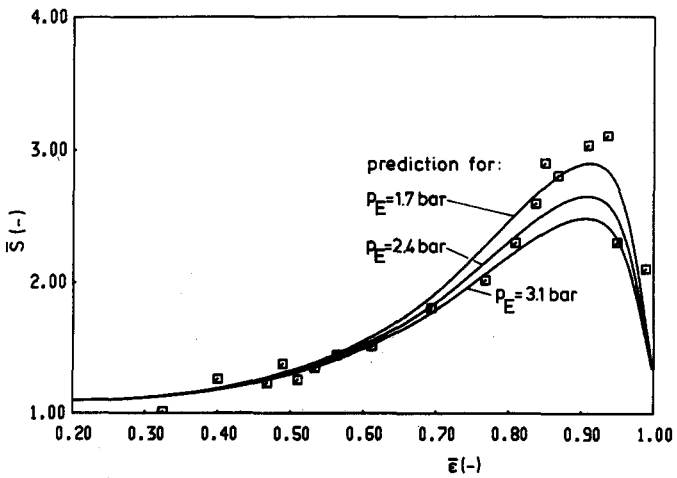

Figure 14. Mean critical velocity ratio (□ $p_E = 1.7 \pm 0.15$ bar, $D = 0.003$ and 0.005 m, $L/D \geq 156$, $T_E \sim 293$K).

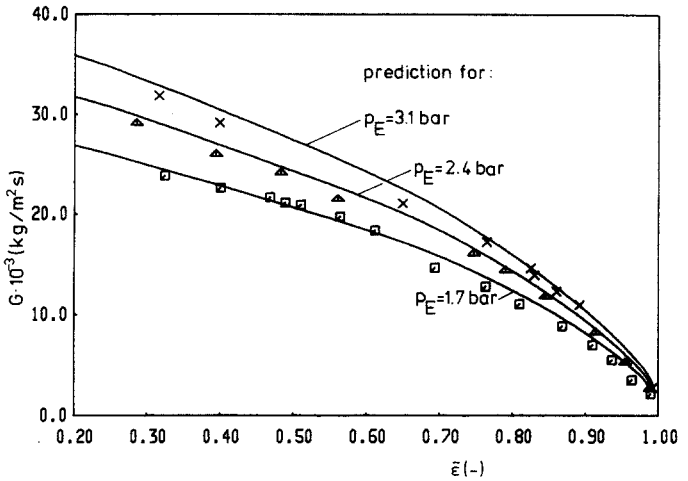

Figure 15. Critical mass flux (□ $p_E = 1.7 \pm 0.15$ bar, △ $p_E = 2.4 \pm 0.2$ bar, × $p_E = 3.1 \pm 0.25$ bar, $D = 0.003$ and 0.005 m, $L/D \geqslant 156$, $T_E \sim 293$K).

distribution equals that in critical flows, but it is not possible to calculate the mean velocity ratio in the same way since the radial velocity distribution is unknown.

Computation of the mean critical velocity ratio and the mean void fraction proved that the relations for the mean void fraction given by Hughmark (1962) and Nabizadeh-Arahgi (1977) are very useful for the evaluation of the present experimental data. The same holds true for the correlations of the frictional pressure loss presented by Beattie & Whalley (1982) and Vinš (1985), and for a homogeneous model published by Friedel (1978). Winter & Deichsel (1988), furthermore, showed that the present concept developed for the description of critical air–water flows can also be applied to liquid–vapor single-component flows, provided their properties and sonic velocities are known. Both, the mean velocity ratio and the critical mass flux were obtained by integration over the flow cross-section in a pipe, but it should also be feasible to adapt this procedure to critical flows in conduits of different shapes.

10. PARAMETER VARIATION

A comprehensive parameter variation was performed in order to prove the applicability of the novel model to the prediction of critical two-phase flow conditions. The sensitivity with which, both, the mean critical velocity ratio, $\bar{S}$, and the critical mass flux, G respond to a variation in the most influential parameters was investigated. Typical results of the study are delineated in figures 16 and 17, the current predictions are drawn in bold lines.

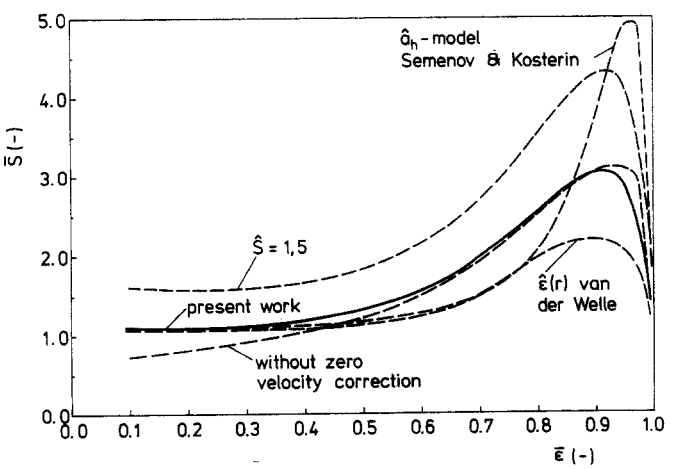

Figure 16. Influence of parameter variation on mean critical velocity ratio ($p_E = 1.4$ bar, $T_E = 293.15$K).

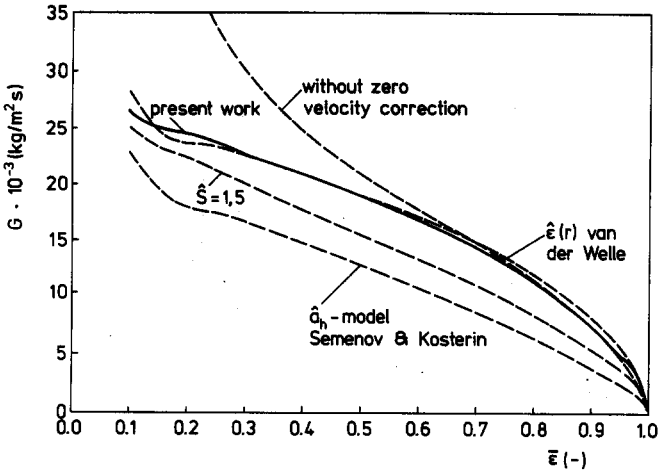

Figure 17. Influence of parameter variation on critical mass flux ($p_E = 1.4$ bar, $T_E = 293.15$K).

If the flow conditions of zero velocity at the wall is relaxed and, furthermore, an increase in the local two-phase velocity in the axial direction between the center of the flow and the wall is permitted, then for void fractions $\bar{\varepsilon} < 0.4$, the current model yields values significantly < 1 for the mean velocity ratio and too large values for the critical mass flux, which are not corroborated by the experiments. In figures 16 and 17 these curves are identified by the notation "without zero velocity correction".

Assuming a local velocity ratio or even a velocity ratio distribution > 1 across the flow in [12] leads to higher mean velocity ratio values than those predicted, causing simultaneously a sizeable decrease in the critical mass flux shown in figures 16 and 17 for a constant local velocity ratio of $\hat{S} = 1{,}5$.

The model for the homogeneous two-phase flow sonic velocity given by Semenov & Kosterin (1964) yields excessively large values for the mean velocity ratio, especially in the range of large void fractions. This behavior of the mean velocity ratio is accompanied by a large decrease in the critical mass flux.

Good agreement, especially in the case of the critical mass flux, between the predictions of the present work and those obtained using van der Welle's (1985) radial distributions of the local void fractions is obtained, when the fact that the local void fraction can not exceed unity is taken into account when performing the computations.

Minor variations in the most significant and interdependent influential parameters show the sensitivity of the present model. In many cases, not all shown here, these variations result in situations which do not reproduce the findings of the experiments and for which no physically meaningful interpretation is possible, hence confirming the applicability and validity of the novel model.

11. CONCLUSIONS

An experimental facility has been designed and constructed for the investigation of critical two-phase flow phenomena in air–water mixtures. Measurements of the total momentum and local total pressure of the flow in the exit cross-sections of various test tubes were conducted. Based on these measurements the interdependence between the mean critical velocity ratio and the local void fractions and velocities could be clarified, revealing a value of 1 for the local velocity ratio, $\hat{S} = 1$ in dispersed critical air–water two-phase pipe flows. For the predetermination of the radial phase distributions, limiting values for the local void fraction in the center of the flow and at the wall of the pipes, as well as a partition exponent, were found for critical dispersed flows in test tubes with i.d. $\geqslant 3$ mm and with length-to-diameter ratios $\geqslant 156$. Applying these radial phase distributions together with a well-known homogeneous sonic velocity model and taking into account the condition of zero velocity at the wall, the mean critical velocity ratio and mass flux were computed with the help of the novel integrational procedure. The results of a brief parameter variation

demonstrate the applicability of the current model to the description of dispersed critical two-phase flows.

REFERENCES

ADORNI, N., CASSAGRANDE, I., CRAVAROLO, L., HASSID, A. & SILVESTRI, M. 1961 Experimental data on two-phase adiabatic flow: liquid film thickness, phase and velocity distribution, pressure drops in vertical gas–liquid flow. C.I.S.E. Report R 35.

BEATTIE, D. R. H. & WHALLEY, P. B. 1982 A simple two-phase frictional pressure drop calculation method. *Int. J. Multiphase Flow* **8,** 83–87.

BEHRINGER, K. 1936 The flow of liquid–gas mixtures in vertical tubes. *Z. ges. Kälteind.* **43,** 55–58.

FALETTI, D. W. 1959 Two phase critical flow of steam water mixtures. Ph.D. Thesis, Univ. of Washington, Seattle, Wash.

FRIEDEL, L. 1978 Druckabfall bei der Strömung von Gas/Dampf-Flüssigkeitsgemischen in Rohren. *Chemie-Ingr.-Tech.* **50,** 167-180.

GIFFEN, E. & CRANG, R. N. 1946 Steam flow in nozzles: velocity coefficient at low steam speeds. 6th Report. *Proc. Instn mech. Engrs* **215.**

HUGHMARK, G. A. 1962 Holdup in gas–liquid flow. *Chem. Engng Prog. Bd* **58,** 62–65.

KLINGEBIEL, W. J. 1964 Critical flow slip ratios of steam water mixtures. Ph.D. Thesis, Univ. of Washington, Seattle, Wash.

KLINGEBIEL, W. J. & MOULTON, R. W. 1971 Analysis of flow choking of two-phase, one-component mixtures. *AIChE Jl* **77,** 383–390.

LANGNER, H. 1978 Untersuchung des Entrainment-Verhaltens in stationären und transienten zweiphasigen Ringströmungen. Diss., TU Hannover.

NABIZADEH-ARAHGI, H. 1977 Modellgesetze und Parameteruntersuchungen für den volumetrischen Dampfgehalf in einer Zweiphasenströmung. Diss., TU Hannover.

NGUYEN, D. L. & WINTER, E. R. F. 1981 Sonic velocity in two-phase systems. *Int. J. Multiphase Flow* **7,** 311.

PETRICK, M. 1962 A study of vapour carryunder and associated problems. Report ANL-6581.

PETRY, G., WINTER, E. R. F. & GREINER, M. 1984 Two-phase critical flow of subcooled freon R-12 in capillary tubes. Presented at the *CHISA Congr.*, Prague.

REIMAN, J. 1983 Developments in two phase mass flow rate instrumentation. In *Advances of Two Phase Flow and Heat Transfer* (Edited by KAKAC, S. & ISHII, M.) Nijhoff, The Hague.

SEMENOV, N. I. & KOSTERIN, S. I. 1964 Results of studying the speed and sound in moving gas–liquid systems. *Teploenergetica* **11,** 46–51.

VANCE, W. H. 1962 A study of slip ratios for the flow of steam–water-mixtures at high void fractions. Ph.D. Thesis, Univ. of Washington, Seattle, Wash.

VAN DER WELLE, R. 1985 Void fraction, bubble velocity, and bubble size in two-phase flow. *Int. J. Multiphase Flow* **11,** 317–345.

VINŠ, L. 1985 Zweiphasenströmung in waagerechten und senkrechten Rohren. Transcript of a seminar presentation at TU München.

WINTER, E. R. F. & DEICHSEL, M. 1988 Experimentelle und analytische Untersuchung adiabater kritischer Wasser/Luft-Zweiphasenströmungen in Rohren kleiner Durchmesser. DFG-Bericht TB 88/1, TU München.

ZUBER, N. & FINDLEY, J. A. 1965 Average volumetric concentration in two-phase flow systems. *Trans. ASME* 453–368.